

Dynamical nuclear polarization for dissipation-induced entanglement in NV centers

Shishir Khandelwal,¹ Shashwat Kumar,² Nicolas Palazzo,² Géraldine Haack,¹ and Mayeul Chipaux^{2,*}

¹*Département de Physique Appliquée, Université de Genève, 1211 Genève, Switzerland*

²*Institute of Physics, École Polytechnique Fédérale de Lausanne (EPFL), Lausanne CH-1015, Switzerland*

(Dated: July 13, 2023)

We propose a practical implementation of a two-qubit entanglement engine which denotes a scheme to generate quantum correlations through purely dissipative processes. On a diamond platform, the electron spin transitions of two Nitrogen-Vacancy (NV) centers play the role of artificial atoms (qubits), interacting through a dipole-dipole Hamiltonian. The surrounding Carbon-13 nuclear spins act as spin baths playing the role of thermal reservoirs at well-defined temperatures and exchanging heat through the NV center qubits. In our scheme, a key challenge is therefore to create a temperature gradient between two spin baths surrounding each NV center, for which we propose to exploit the recent progresses in dynamical nuclear polarization, combined with microscopy super-resolution methods. We discuss how these techniques should allow us to initialize such a long lasting out-of-equilibrium polarization situation between them, effectively leading to suitable conditions to run the entanglement engine successfully. Within a quantum master equation approach, we make theoretical predictions using state-of-the-art values for experimental parameters. We obtain promising values for the concurrence, reaching theoretical maxima.

I. INTRODUCTION

The generation of quantum entanglement is a crucial task for quantum information processing. Typically, this requires performing logical two-qubit unitary operations and limiting the quantum systems' interaction with their environment

These implementations require isolating the quantum systems from their environment, and platform-dependent techniques have been developed to achieve that, for superconducting circuits [1] and trapped ions [2], for instance. However, avoiding all possible sorts of uncontrolled dissipation processes is impossible. In this context, natural questions arise. Is it possible to exploit dissipation with thermal environments to create quantum resources? And how could this be implemented? In recent years, those questions have triggered number of theoretical works, leading to proposals for realizing thermal machines generating quantum correlations [3–9]. It has also been demonstrated that the generated entanglement can be useful for performing non-classical operations [10, 11]. However, experimental demonstrations of these ideas are still lacking. In this work, we propose an experimental implementation of a two-qubit entanglement engine on a Nitrogen-Vacancy (NV)-center platform.

NV centers found in diamond are recognized as one of the most promising platforms for quantum technologies. As first demonstrated in 1997 [12], they possess the features of an Optically Detected of Magnetic Resonance (ODMR) system [13]. This means that their electron-spin, coherently controlled with microwave, can be initialized and read-out with optical means. In practice, this is performed with standard microwaves and visible

range photo-luminescence microscopy equipment in the visible range [14], or through Ground State Depletion (GSD) [15] or STimulated Emission Depletion (STED) [16] for better resolution. Combined with remarkable room-temperature quantum properties [17], these qualities make NV centers particularly successful for quantum sensing applications [18–20], while allowing for very versatile experimental conditions such as high pressure [21] or high temperature [22] conditions or within biological environments [23].

NV centers also constitute a promising platform for quantum information processing [24, 25]. Their fine and hyperfine structure with surrounding electronic or nuclear spins give them numerous controllable quantum degrees of freedom. Notably, NV centers can be exploited to control and entangle the dark electronic and nuclear spins of nearby P1 centers (corresponding to a nitrogen substitution) [26]. They are also often used as quantum bus to control multiple surrounding Carbon-13 (¹³C) nuclear spins operating as quantum memories [27]. In parallel, Dynamical Nuclear Polarization (DNP) techniques [28–30] have been developed to control the state of nuclear spins which are near the NV centers. These nuclear spins can be located in the bulk or at the surface of the diamond, and can correspond to different elements (¹³C, ¹⁹F or ¹H). These techniques were primarily developed towards hyperpolarized Nuclear Magnetic Resonance (NMR) applications [31]. From the perspective of open quantum systems, they constitute a path to realize effective spin baths with specific properties that can be controlled through the NV centers.

In this work, we exploit recent developments in the field of NV centers to propose an experimental scheme for a thermal machine to produce entanglement between the electronic spins of two NV centers. Towards this goal, we put forward a novel application of DNP techniques to engineer two effective spin baths characterized by distinct polarizations. This also enters a broader field of appli-

* Correspondence: mayeul.chipaux@epfl.ch

cations that may require the control of the heat flow in NV-center technologies.

The article is organized as follows. In Sec. II, we briefly recall the basic ingredients of an entanglement engine to achieve dissipation-induced entanglement between two artificial atoms. In Sec. III, we propose the electronic spin of an NV center to play the role of an artificial atom, elaborating upon the various energy scales involved and the conditions to be satisfied to have steady-state entanglement between the electronic spins. In Sec. IV, we discuss how these electronic spins can be made to interact with their surrounding ^{13}C nuclear spin bath and show how a cross-relaxation regime may allow for purely dissipative dynamics. In Sec. V, we tackle the main challenges of this proposal, namely the realization of two thermal environments biased in temperature, combining dynamical nuclear polarization (DNP) techniques with microscopy superresolution methods. In Sec. VI, we finally predict the presence of dissipation-induced entanglement between two NV centers using realistic theoretical predictions as well as state-of-the-art experimental parameters.

II. THEORETICAL MODEL

A minimal model to investigate entanglement generation from dissipation is made of two interacting artificial atoms (qubits), each of them being tunnel-coupled to a thermal environment. These environments are assumed to be independent from one another, well-defined by their respective temperature and chemical potential through their Fermi distribution. When subject to a bias in temperature, a heat current flows between the two environments, through the system. If the qubits are interacting through a flip-flop type Hamiltonian (see below), this heat current has been demonstrated to sustain the presence of entanglement in the steady-state regime [3, 6, 32] and proposals were developed for semiconducting and superconducting platforms [8, 9]. We now briefly recall the Hamiltonian of the two interacting qubits in this model, as well as the master equation that will be used to investigate the dynamics of this entanglement engine.

The Hamiltonian of the two qubits is given by,

$$H_S = \varepsilon_L \sigma_L^+ \sigma_L^- \otimes \mathbb{1}_R + \mathbb{1}_L \otimes \varepsilon_R \sigma_R^+ \sigma_R^- + g(\sigma_L^+ \otimes \sigma_R^- + \sigma_L^- \otimes \sigma_R^+), \quad (1)$$

where ε_α ($\alpha = \text{L, R}$) are the energies of the left (L) and right (R) qubits and g is the strength of the inter-qubit coupling. The raising and lowering operators for qubit α are respectively σ_α^+ and σ_α^- . For a two-qubit device, it has been shown that a flip-flop type interaction Hamiltonian is suitable for entanglement generation [3, 6]. The qubits are distinctly coupled to two fermionic reservoirs (the choice is suitable for the NV-center platform, as we explain below). Assuming Markovian dynamics and weak system-reservoir couplings, the dissipative dynamics of the qubits can be described by a Lindblad master

equation. Furthermore, if the interaction g , is small in comparison to ε_α , the following local master equation is consistent [33],

$$\dot{\rho}(t) = -i[H_S, \rho(t)] + \sum_{\alpha \in \{\text{L, R}\}} \gamma_\alpha^+ \mathcal{D}[\sigma_\alpha^+] \rho(t) + \gamma_\alpha^- \mathcal{D}[\sigma_\alpha^-] \rho(t), \quad (2)$$

with the dissipators defined as $\mathcal{D}[A] \rho(t) := A \rho(t) A^\dagger - \{A^\dagger A, \rho(t)\}/2$ and σ_α^\pm the raising and lowering operators. In case of fermionic baths, the Fermi distribution $n_F(\varepsilon_\alpha, T_\alpha)$ characterizing the environment of qubit α is evaluated at the qubit's energy ε_α and temperature T_α . The total coupling rates are the product of the bare rate Γ_α (which depend on the microscopic details of the platform) and of the occupation probability of the environment [34],

$$\begin{aligned} \gamma_\alpha^+ &= \Gamma_\alpha n_F(\varepsilon_\alpha, T_\alpha) \\ \gamma_\alpha^- &= \Gamma_\alpha (1 - n_F(\varepsilon_\alpha, T_\alpha)). \end{aligned} \quad (3)$$

A temperature gradient between the two baths, $T_L \neq T_R$, induces a heat current flowing through the system. It was shown in [3, 6] that, above a certain threshold for the heat current, entanglement between the two qubits is present in the steady state, but also in the transient regime. In the following sections, we discuss how to realize this model on a NV-center platform; first showing how the coupling between the NV-center qubits can be realized, and then showing how an effective temperature (polarization) gradient between the qubits can be created.

III. REALIZATION OF THE SYSTEM HAMILTONIAN

A. The diamond NV center

The NV center's optical ground state is spin triplet. The degeneracy between the non-zero states can be lifted in the presence of a magnetic through the Zeeman effect [35]. Interestingly, the spin state can be initialized by an off-resonance optical green pump (e.g. 520 or 532 nm) and read-out through its red photo-luminescence (from 600 to 800 nm). With $\vec{S} = \{S_x, S_y, S_z\}$ the NV-center electronic spin and m_S the associated spin quantum number, the NV center ground state Hamiltonian in a magnetic field \vec{B} (Fig. 1) can be written as,

$$H_{NV} = DS_z^2 + \gamma_e \vec{B} \cdot \vec{S} + H_N + H_T, \quad (4)$$

where the constant $D = 2\pi \times 2.87 \text{ GHz}$ is the Zero Field Splitting (ZFS) and $\gamma_e = g\mu_B/\hbar = 2\pi \times 28.0 \text{ GHz T}^{-1}$ is the electronic-spin gyromagnetic ratio. H_N and H_T describe the hyperfine interaction of the NV center electronic spin \vec{S} with the nitrogen atom (^{14}N or ^{15}N), and

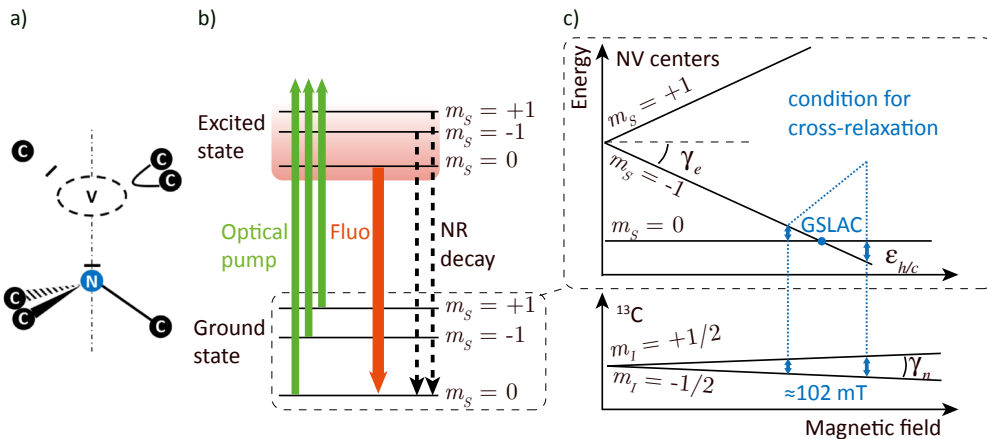


FIG. 1. a) A representative sketch of a NV center in diamond; the Nitrogen atom “N” next to the vacancy “V”, in a diamond lattice made of Carbon C. The electrons are shown in the Cram representation for 3 dimensional aspects. b) NV center spin-conservative electronic and optical transitions. The NV center is pumped by a green laser (typically at 532 nm) and emits a red broadband photo-luminescence. A non-radiative decay path allows for spin non conservative transition and a polarization of the NV centers to its state of null spin. c) Energy diagram as a function of an aligned magnetic field. At certain magnetic field values, the transition of the NV center $m_s = 0 \leftrightarrow m_s = -1$ may be at resonance with the one of the $^{13}\text{C} -1/2 \leftrightarrow +1/2$. This corresponds to the cross-relaxation condition.

the surrounding ^{13}C (see Sec. IV). B_{\parallel} and B_{\perp} are respectively the longitudinal and the transverse components of the magnetic field with respect to the NV center quantization axis ($N - V$) joining the nitrogen to the vacancy. The eigenenergies of the NV center corresponding to the spin states $|m_s = \pm 1\rangle$ can be controlled through B_{\parallel} according to the following equation [36], up to first order in B_{\perp} (see hereafter), $\varepsilon_{\pm}(B_{\parallel}) = D \pm \gamma_e B_{\parallel}$. In the following, we consider the energy transition from the ground state to the lowest excited state $|m_s = -1\rangle$ as the qubit transition, see top panel in Fig.1 c),

$$\varepsilon_{L,R} \equiv \varepsilon_{-} = D - \gamma_e B_{\parallel}. \quad (5)$$

To realize Hamiltonian of Eq. (1), and the system evolution according to Eq. (2), it is essential that the two electronic spins are resonant not only with each other, but also with the nuclear spins of the surrounding ^{13}C . Under the assumption of a parallel magnetic field only, the energy of the nuclear spins of the ^{13}C is simply given by,

$$\varepsilon_n = \gamma_n B_{\parallel}. \quad (6)$$

The resonance condition imposes a condition on the modulus of the magnetic field to be close to the Ground State Level Anticrossing (GSLAC) condition,

$$\varepsilon_{L,R} = \varepsilon_n \quad (7)$$

$$\Leftrightarrow D - \gamma_e B_{\parallel} = \gamma_n B_{\parallel} \quad (8)$$

$$\Leftrightarrow B_{\parallel} \equiv B_{CR} = D/(\gamma_e + \gamma_n) \approx 102 \text{ mT}. \quad (9)$$

For estimating B_{CR} , we have assumed $\gamma_n \ll \gamma_e$, valid for any nuclear spin with respect to any electronic spin. The label CR for the magnetic field ensuring Eq. (7) refers

to the energy-resonance condition, known as the cross-relaxation regime [37, 38].

The energy-resonance regime must be reached while preserving the NV centers’ quantization axes and their ODMR properties [39]. This imposes that the applied magnetic field must be well aligned with the quantization axis ($N - V$) of the two qubits, hence $B_{\perp} \approx 0$ as in Eq. (5). Subsequently, this also imposes that the two NV centers are along the same crystallographic orientation, aligned with the magnetic field. In Fig. 1, we provide a schematic view of a NV center, its electronic and optical transitions, as well as the energy diagram with the key conditions to satisfy with the applied magnetic field.

We now discuss the additional terms H_N and H_T in Eq. (4). Near GSLAC, H_N plays an important role which depends on the type of nitrogen isotope used in the experiment [40, 41]. As shown in Ref. [37], the energy transition between states $|m_s = 0\rangle$ and $|m_s = -1\rangle$ of a NV center comprising of the spin doublet ^{15}N isotope cannot be lowered below 2 MHz and reach the ^{13}C nuclear transition. This makes ^{15}NV unsuitable for our proposal. Instead, the nuclear triplet ^{14}N , naturally much more abundant ($> 99.5\%$) than the other isotopes, satisfies this condition and will be considered here. As discussed in detail in Sec. IV, this isotope has already been demonstrated to reach the cross-relaxation regime with ^{13}C [28] and other nuclear spins of higher gyromagnetic ratio [38]. Finally, with I_n the nuclear spin operator and m_I its associated spin quantum number, close to GSLAC, the ^{14}N center nuclear spin is naturally polarized into its non-interacting $|m_I = 0\rangle$ state in a durable manner [41, 42], which explains the absence of role played by H_T in this regime.

B. Inter-qubit dipole-dipole interaction

The electronic spins of two NV centers interact naturally through a dipole-dipole interaction, whose strength depends on the electromagnetic gyromagnetic ratio γ_e of each NV center and on the relative distance between them characterized by the vector $\vec{r} = r\hat{e}_r$ below. Within the secular approximation (valid at high magnetic field), the dipole-dipole interaction Hamiltonian takes the form [43, 44],

$$H_{LR} = \frac{\mu_0\gamma_e\gamma_e\hbar}{4\pi r^3}(1 - 3\cos^2\theta) \left(S_L^z S_R^z - \frac{1}{4}(S_L^+ S_R^- + S_R^+ S_L^-) \right), \quad (10)$$

where the first two terms correspond to the terms A and B of the dipolar alphabet of the dipole interaction Hamiltonian. Let us note that, for clarity, we have omitted the tensor product in the above equation compared to Eq. (1). In the literature, the case of two off-resonant nuclear spins is typically discussed such that the second term is neglected. In this proposal, we consider the regime of resonant nuclear spins for which the Hamiltonian above should be considered [45]. In particular, one notes that the second interaction term realizes the flip-flop interaction required by Eq. (1) with the coupling constant g set by,

$$|g| = \frac{\mu_0\gamma_e^2\hbar}{4\pi r^3} \frac{1 - 3\cos^2\theta}{4}. \quad (11)$$

The angle θ denotes the angle between the orientation NV-center axis and the direction of B_{\parallel} (B_{CR}). The contribution of the $S_L^z S_R^z$ term only plays a role for a certain class of initial states, those who are not described by a X -shaped density operator. The predictions we make in the following sections are done considering relevant experimental initial states, which are all of a X -shape. For other initial states, this term will induce additional non-zero off-diagonal terms in the transient regime, but will not affect the steady state. We can therefore neglect this term without loss of generality for this proposal.

For a successful realization of a NV-based entanglement engine, interaction strength g must within the right energy range with respect to bare energies of the NV centers and relaxation rates Γ_{CR} with the surrounding ^{13}C (discussed just below), $\Gamma_{\text{CR}} \leq g \ll \varepsilon$. The interaction strength g directly depends on the distance between the two NV centers. In recent years, stochastic implementation of pairs [46–48] and triplets [49] of NV centers has been achieved in experiments. The implantation energy determines the final depth and straggling [50] of the nitrogen atoms in the diamond, and therefore the expected distance that separates them. Based on magnetic spectroscopy measurements, coupling strengths ranging from a few kHz as limited by decoherence, up to the record of 3.9 MHz reported in Ref. [47] have been demonstrated, falling well into the above range. The main experimental

values of the parameters of the model that correspond to the discussions in the present and following sections are summarized in Table I.

We now discuss environment engineering and relaxation energy scales.

IV. SYSTEM-ENVIRONMENT INTERACTION

In this section, we first discuss the role of different environments for an NV center and then propose a scheme to engineer an out-of-equilibrium situation between two NV centers, which is required for entanglement generation.

A. Dipolar interaction

A key advantage of the NV-center platform is the excellent decoupling of NV centers from lattice phonons [51], with a room temperature spin-lattice relaxation rate as low as a few hundreds of Hertz. As a consequence, quantum coherence properties of NV centers are mainly limited by surrounding magnetic impurities ^{13}C in our case [17, 19, 52, 53].

The interactions between a NV center's electronic spin α , and the j -th ^{13}C 's nuclear spin is again described by the dipole-dipole Hamiltonian. Within the secular approximation, under resonant conditions discussed in Eqs. (7) and (9), the electronic spin α (with gyromagnetic ratio γ_e) interacts with N ^{13}C nuclear spins (with gyromagnetic ratio γ_n) with the Hamiltonian $H_{T,\alpha}$,

$$H_{T,\alpha} = \sum_{j=1}^N \frac{\mu_0\gamma_e\gamma_n\hbar}{4\pi r_{\alpha j}^3} (1 - 3\cos^2\theta_{\alpha j}) \left(S_{\alpha}^z I_j^z - \frac{1}{4}(S_{\alpha}^+ I_j^- + I_j^+ S_{\alpha}^-) \right). \quad (12)$$

Here, $\vec{S}_{L,R}$ and \vec{I}_j denote the spin and nuclear operators respectively. The term $S_{\alpha}^z I_j^z$ will lead to pure dephasing via the rate $\Gamma_{2,\varphi}$ of the electronic spin of the NV centers, while the tunneling (flip-flop) term is at the origin of dissipation (decoherence rate $\Gamma_{2,\text{CR}}$ and relaxation rate $\Gamma_{1\alpha}$). In the following subsections, we discuss in further detail these rates and predicted values in the context of our proposal.

B. Cross-relaxation rate

The effect of the ^{13}C nuclei on the relaxation of the NV center α is known to be determined by the product of the root mean squared value of the transverse magnetic field noise, $B_{\text{rms},\alpha}$, and its spectral density $S_{\alpha}(\varepsilon)$ [43, 54],

$$\Gamma_{1,\alpha}(\varepsilon) = 3\gamma_e^2 (B_{\text{rms},\alpha})^2 S_{\alpha}(\varepsilon). \quad (13)$$

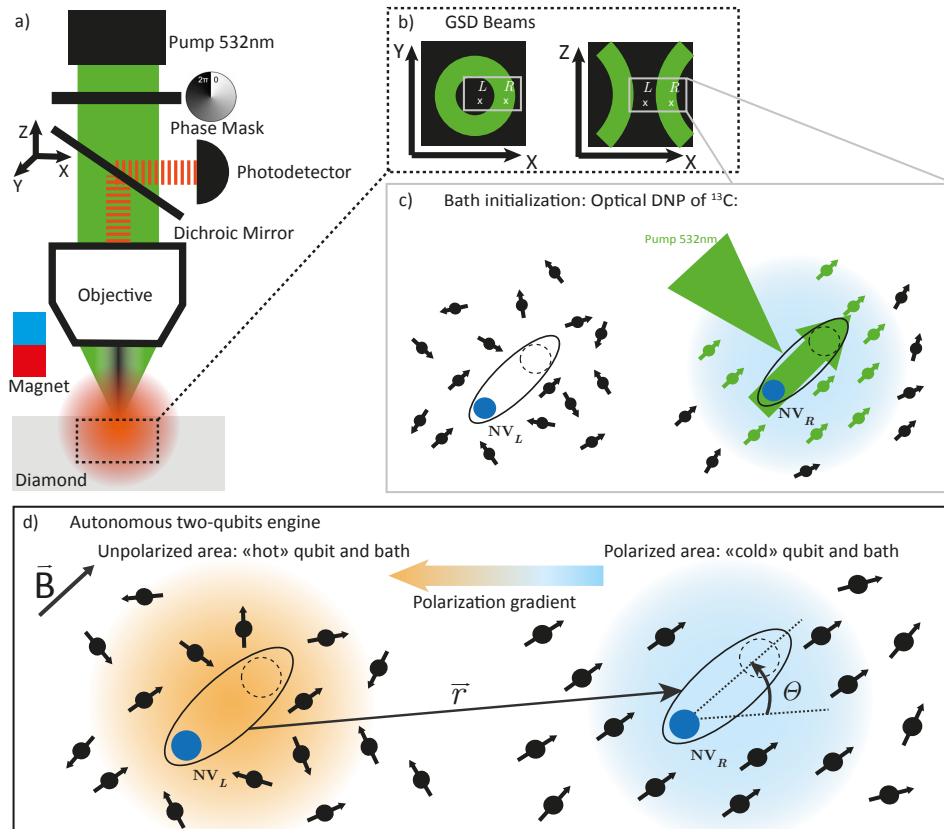


FIG. 2. a) Experimental setup with ground state depletion capabilities. b) Pumping beam profile at the system level. c) Dynamical Nuclear Polarization on one NV center, cooling the surrounding ^{13}C spin bath. d) Configuration of the autonomous two-qubit entanglement engine, with the optical pumping beam off.

In full generality, the spin-lattice relaxation rate Γ_{SL} needs to be added to this expression, if non-negligible. Considering the contributions of all ^{13}C nuclei to be independent from each other, $(B_{\text{rms},\alpha})^2$ can be obtained by summing up all the contributions squared [43],

$$(B_{\text{rms},\alpha})^2 = \sum_j \left(\frac{\mu_0 \gamma_n \hbar}{4\pi} \right)^2 C_S \frac{2 + 3 \sin^2 \theta_{\alpha j}}{r_{\alpha j}^6}, \quad (14)$$

where $C_S = 1/4$ is linked to the multiplicity of the reservoir spins. The number of nuclear spins contributing to the sum over j can be estimated through the volume of influence [55]. Nuclear spins that are closer than a minimal radius around the NV center $R_m \approx 0.2$ nm, as well as the ones beyond a maximal radius $R_M \approx 1.33$ nm are excluded. In a diamond with a natural abundance of ^{13}C of $n_C = 1.1\%$, we estimate the sum over j to comprise approximately 20 spins, which will define the environment of the electronic spin of NV center α . Assuming $r_{\alpha j} = r_\alpha$ and the same orientation of the nuclear spins with respect to the quantization axis of spin α , $\theta_{\alpha j} = \theta_\alpha$, Eq. (14) can then be written as,

$$\begin{aligned} (B_{\text{rms},\alpha})^2 &= C_S \left(\frac{\mu_0 \gamma_n \hbar}{4\pi} \right)^2 \iiint_{r > R_m} \frac{2 + 3 \sin^2 \theta_\alpha}{r^6} n_C dV, \\ &= C_S \left(\frac{\mu_0 \gamma_n \hbar}{4\pi} \right)^2 \frac{7\pi}{2R_m^3} n_C, \end{aligned} \quad (15)$$

where n_C is the average ^{13}C density, or its natural abundance. The spectral density $S_\alpha(\varepsilon)$ is approximated by a Lorentzian, centered on the nuclear spin energy ε_n (see Eq. (6)), and whose linewidth is limited by the NV center decoherence $\Gamma_{2,\alpha}$ [56, 57],

$$S_\alpha(\varepsilon) = \frac{1}{\Gamma_{2,\alpha}} \times \frac{1}{1 + (\varepsilon - \varepsilon_n)^2 / \Gamma_{2,\alpha}^2}. \quad (16)$$

In the most common off-resonance case ($\varepsilon_\alpha \gg \varepsilon_n$), the spectral density vanishes such that the nuclear spin induced relaxation remains small with respect to the spin lattice one.

Instead, in the cross relaxation condition which applies here ($\varepsilon_{L,R} = \varepsilon_n$), the maximal relaxation rate, hereby called cross-relaxation rate, has the form:

$$\Gamma_{1,\text{CR}}^\alpha = \frac{3\gamma_e^2 (B_{\text{rms}}^\alpha)^2}{\Gamma_{2,\alpha}}. \quad (17)$$

It has been measured up to $\Gamma_{1,\alpha} = 250$ kHz in a diamond with a natural concentration of ^{13}C [28], three orders of magnitude larger than the spin-lattice relaxation rate 200 Hz in the same sample.

For our proposal, considering the natural abundance n_C , the cross-relaxation bare rate Γ_α in Eq. (3) will be taken to be,

$$\Gamma_1 \equiv \Gamma_{1,\alpha} (\%(^{13}\text{C})) = \frac{\%(^{13}\text{C})}{1.1\%} \times 250 \text{ kHz}. \quad (18)$$

In a similar sample diamond, the decoherence rate is measured to be of the order of 1.5 kHz [52], with a linear increase with n_C :

$$\Gamma_{2,\alpha} (\%(^{13}\text{C})) = \frac{\%(^{13}\text{C})}{1.1\%} \times 1.5 \text{ kHz}, \quad (19)$$

This remains two order of magnitude lower than the relaxation rate. In the cross relaxation regime, the dynamics of the NV centers' electron spins can therefore be modeled by the purely dissipative cross-relaxation process, for which Eq. (2) should be valid. In the following, we consider the same bare rates for the electronic spins coupled to their respective nuclear spin baths, $\Gamma_L = \Gamma_R = \Gamma_1$ given by Eq. (18).

V. THERMALLY BIASED ENVIRONMENTS

In this section, we explain how to engineer two artificial thermal environments made of ^{13}C nuclear spins, biased in temperature. In an NV-center platform, this is made possible owing to the NV centers being naturally decoupled from the phonons [51], allowing us to not be subject to the excellent thermal conduction properties of the diamond. Here, we realize an effective temperature difference between two ensembles of nuclear spins through Dynamical Nuclear Polarization (DNP). We predict this technique to enable a long lasting out-of-equilibrium situation within the context of this proposal. The main steps are shown in Fig. 2 and discussed below.

A. Dynamical Nuclear Polarization

For the nuclear spins with energy ε_n within the volume of influence of each NV center (at a position \vec{r} and time t), it is possible to estimate their polarization $p = p_\downarrow - p_\uparrow$ by assuming a Boltzmann distribution for each of the nuclear spin state $p_\downarrow = 1/(e^{-\varepsilon_n/(k_B T)} + 1)$ and $p_\uparrow = 1 - p_\downarrow$,

$$p = p_\downarrow - p_\uparrow = \frac{1 - e^{-\varepsilon_n/k_B T}}{1 + e^{-\varepsilon_n/k_B T}} \quad (20)$$

At room temperature, with $\varepsilon_n = 1.1$ MHz and $B_{\text{CR}} = 102$ mT, we obtain $p \approx 10^{-7}$, corresponding to a situation without any effective temperature gradient.

Several methods have been proposed and experimentally demonstrated to lower or increase the polarization

of nuclear spins by transferring the polarization of an electronic spin in their vicinity. These techniques are known as Dynamical Nuclear Polarization (DNP). With NV centers, a common technique is the Hartmann-Hahn (HH) protocol [58], which drives the electron and nuclear spins in a synchronous manner. It has been adapted to the NOVEL sequence [30, 59], using spin locking to adjust the Rabi frequency in the rotating frame to the nuclear Larmor frequency, or to the more recent PulsePol schemes [29, 60]. In the cross-relaxation regime, which is relevant for this proposal, no radio frequency fine tuning is necessary; DNP is achieved through optical pumping of the NV center. Recently, a cross-relaxation induced polarization (CRIP) protocol has demonstrated a polarization as high as 99% for ^{13}C and FI [28]. DNP uses the NV center as a source of polarization via the spin selective non-radiative decay path, which allows the preparation of a nuclear target spin into its $|m_S = 0\rangle$ state [12]. While polarization of a single nuclear spin through DNP is estimated to happen in tens of ns, it was shown experimentally that polarization of nuclear spins within the volume of influence of a NV center takes of the order of a few μs [59].

DNP protocols are therefore foreseen to be suitable to cool down nuclear spins within the volume of influence of a given NV center, hence realizing an effective thermal bath characterized by an effective temperature that is lower than room temperature. A remaining challenge for our proposal is the ability to select the NV center for applying DNP, i.e. to achieve a selective cooling. We discuss this below.

B. Selective cooling

To achieve selective cooling of nuclear spins surrounding a given NV center, we envision two possible experimental schemes.

The first involves distinguishing the two thermal baths by their electron paramagnetic spectrum [61]. A ^{13}C nuclear spin close to one NV can shift its resonance such that a DNP protocol could target it specifically. This however would involve having qubits of different energies which is less favorable to generate entanglement; see [6] for theoretical predictions. Another approach, shown in Fig. 2, involves using a superresolution microscopy method such as Ground State Depletion (GSD) [15] or STimulated Emission Depletion (STED) [16]. In the case of GSD, the pumping beam (green) is patterned to have a central dark spot on the focus plane (see Fig. 2b)). The NV center within the dark spot is therefore not optically pumped while the other is. In the case of STED, a similarly patterned depletion beam [16] is added to a conventional green pump. The NV center placed in the dark center of that red beam is pumped normally, while the excited state of the other NV center is depleted such that its spin-non conservative decay path is impeached. In either case, only one of the two NV centers can be reg-

ularly pumped and act as a local source of polarization for a DNP protocol.

To summarize, in our proposal, the hot bath is realized by considering the nuclear spins surrounding the left NV center (for instance), the effective hot temperature being the room temperature corresponding to a polarization close to 0. The cold bath will be realized through DNP and selective cooling as discussed above and shown in Fig. 2. The predicted effective cold temperature is estimated through the achieved polarization in the range 97%–100%. With these experimental achievements, the rates entering the Lindblad master equation Eq. (2) for the left (hot) and right (cold) baths can be identified as:

$$\gamma_L^+ = \gamma_L^- = \frac{1}{2} \Gamma_1, \quad (21)$$

$$\gamma_R^- = \frac{1+p_R}{2} \Gamma_1 = (1-n_F(\varepsilon, T_R)) \Gamma_1, \quad (22)$$

$$\gamma_R^+ = \frac{1-p_R}{2} \Gamma_1 = n_F(\varepsilon, T_R) \Gamma_1, \quad (23)$$

with $p_R \in [0.97, 1]$ and Γ_1 given by Eq. (18). Before discussing the numerical predictions for this NV-center based entanglement engine, we comment on spin diffusion and spin-lattice relaxation that would, in general, affect DNP protocols.

C. Spin diffusion

In general, spin polarization in DNP protocols may also happen through spin diffusion, as spins interact directly through the dipole-dipole interaction Hamiltonian (similar to Eq. (10)).

In a 100% enriched diamond, the spin diffusion constant can be calculated directly $D_n(100\%) = 6.5 \text{ nm}^2 \text{ s}^{-1}$. It has a square-root dependence on n_C [62]. For our proposal, we estimate it to

$$D_C(\%({}^{13}\text{C})) = \sqrt{\frac{\%({}^{13}\text{C})}{100\%}} \times 6.5 \text{ nm}^2 \text{ s}^{-1} \quad (24)$$

This is also consistent with the experimental value of $6.5 \text{ nm}^2 \text{ s}^{-1}$ obtained in [55] for a diamond with ${}^{13}\text{C}$ in natural abundance. Another indirect experimental estimation gives a diffusion constant higher by one order of magnitude [63]. However, this is related to a diamond being with additional nitrogen impurities which can mediate the spin diffusion. Accounting for spin diffusion, the polarization of a given bath is expected to propagate over a distance of $d = 20 \text{ nm}$ in $\approx \frac{d^2}{D_C} = 1 \text{ min}$. This time scale is orders of magnitude higher than the other time scales involved in this proposal which are of the order of tens of microseconds (See Fig. 3 panel c)) and previous discussions. We therefore predict this spin diffusion to be negligible in the realization of an entanglement engine.

In the last section, we present numerical estimations for the concurrence, a measure for entanglement. We investigate it as a function of relevant parameters of the

proposal, the polarization of the nuclear spin baths, the concentration of ${}^{13}\text{C}$ and the coupling g between the NV centers, which is determined by the distance between them.

VI. ENTANGLEMENT GENERATION

Having discussed all relevant factors that determine the quantum evolution of the NV centers in our scheme, we now proceed to discuss the dynamics. For this purpose, we take the master-equation approach described in Sec. I. Analytical results on both steady-state [6] and transient regimes [64] have been previously discussed for the system. Here, we focus on numerically demonstrating the generation of entanglement considering values for the parameters that correspond to the techniques and regimes described in the previous sections.

In Fig. 3 panel a), we show the steady-state concurrence [65] as a function of polarization and coupling between the NV centers for natural concentration of ${}^{13}\text{C}$. We find that there is a large range of experimental parameters for which the qubits become entangled in the steady state. Specifically, higher the polarization (i.e., lower the effective temperature of the “cold” reservoir), and larger the coupling between them (i.e., smaller the distance between them), the higher the steady-state entanglement. The entanglement is larger with increasing temperature gradient, but the maximum takes place at an intermediate inter-qubit coupling. The parameter range where entanglement is nonzero can be obtained exactly via the critical heat current introduced in [64].

In general, entanglement may appear in the transient dynamics and may disappear completely at long times. Furthermore, depending on the time-scale of the dynamics of the machine, it may be more experimentally feasible to look at short or intermediate times to detect entanglement. Importantly, the entanglement at an intermediate time may be much larger than at long times. It is therefore, also important to investigate entanglement production in the transient regime. In Fig. 3 panel c), the goal is to see how much entanglement can be created at intermediate times for different concentrations of ${}^{13}\text{C}$ in the diamond sample. In Fig. 3 panel b), for given concentration, we plot the optimal value of g (i.e., the value which maximizes transient concurrence). In Fig. 3 panel c), we use these value of g to plot the concurrence as a function of time. We find that for any given concentration, there is a g , such that concurrence can be maximised to the same value in the transient state, which is more than double the steady-state concurrence. Since g is one of the factors that determines the time scale of the dynamics, this maximum, however, happens at different points in time. Interestingly, in the steady state, all curves approach the same value of concurrence (see inset).

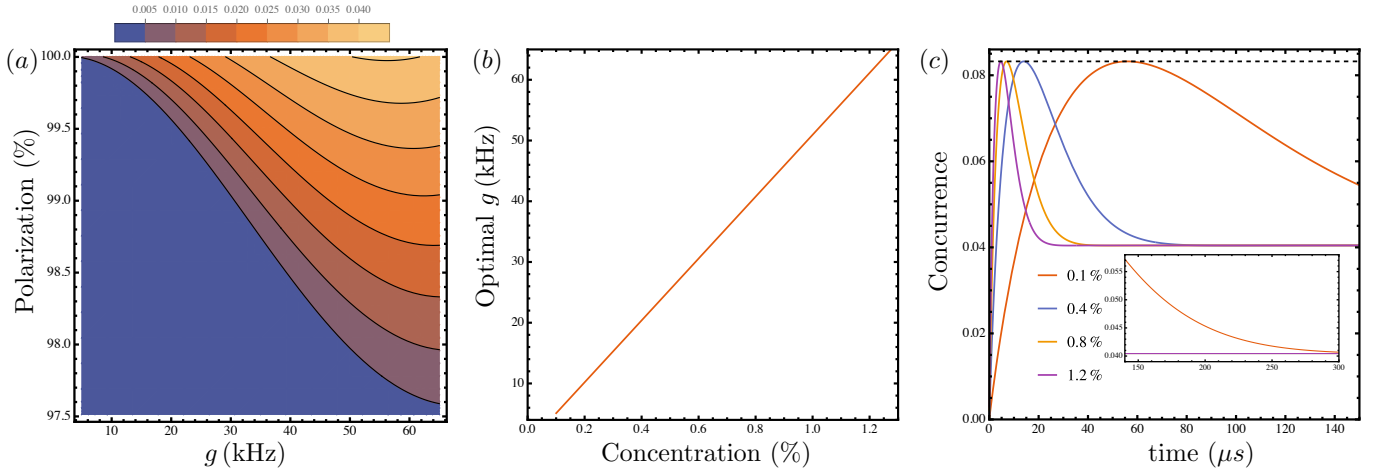


FIG. 3. Entanglement predicted between the two NV centers. a) Contour plot showing the concurrence as a function of the polarization % and the inter-qubit coupling, g . The other parameters are $\varepsilon = 1.1$ MHz, $T_h = 1$ GHz and natural concentration of $^{13}\text{C} = 1.4$ %. b) The optimal values (i.e., optimized to maximize the steady state concurrence) of inter-qubit coupling for given ^{13}C concentrations. c) Transient behaviour of concurrence for four different values of concentration and the corresponding optimal value of inter-qubit coupling. The other parameters are $\varepsilon = 1.1$ MHz, $T_h = 1$ GHz and 100 % polarization of ^{13}C constituting the cold reservoir. The initial state is chosen to be a tensor product of thermal states at the reservoir temperatures (i.e., with $n_F^c = 0$ and $n_F^h \approx 1/2$). The couplings are such that $g < 70 \text{ kHz} < \Gamma_{1,\text{CR}}^{(i)} = 250 \text{ kHz}$, which fits the chosen master equation regime.

VII. CONCLUSION

In this work, we have proposed an experimental setup to realize a two-qubit entanglement engine on an NV-center platform. We discuss the implementation of two interacting qubits, as well as the realization of two independent nuclear spin baths characterized by different temperatures. This temperature gradient is realized effectively through a polarization gradient created using DNP. It is interesting to note that certain DNP protocols can also engineer effective baths at negative temperature [29, 30], corresponding to spin bath polarized in their “up” state. From a thermodynamic point of view, this constitutes an interesting resource, already discussed in few works in the context of quantum thermal machines [10, 67, 68].

A key requirement of a two-qubit engine is to maintain a long lasting out-of-equilibrium situation. In schemes involving local interactions, this appears particularly difficult. It is indeed required to avoid any direct coupling between the two thermal reservoirs, at a similar distance to one another than the one between qubits, while keeping dominating qubits/qubit and qubit/bath couplings with similar order of magnitude. In our scheme, this is made possible by exploiting the large difference between the gyromagnetic moments of, on one side the nuclear spins for the baths and on the other side the electronic spins for the two interacting qubits. For instance, in the alternative of considering baths made of electronic spins, all interaction strengths would be set by the gy-

romagnetic moments of electronic spins, preventing the realization of two independent reservoirs interacting distinctively with each NV center.

As a possible alternative, one may consider different nuclear spins. For instance, in references [29, 30], local efficient polarization of surface nuclear spins ^{19}F or ^1H has been demonstrated. The relevant references and parameters to investigate such configurations together with alternative ^{13}C volume concentrations are provided in Table I. In those cases, one could take profit of the potential shorter distance between nuclei to strengthen the thermal reservoir approximation by involving more of them in each bath enabling interactions between them. The qubit/bath coupling could then be set by the NV centers’ depths. In such cases however, the spin diffusion to be considered may then not be negligible anymore and would required a proper modeling. Such alternatives may constitute interesting schemes to be investigated both theoretically and experimentally.

ACKNOWLEDGEMENTS

The authors thank Christophe Galland and Jonatan Bohr Brask for discussions at an early stage of this work. All authors acknowledge support from the Swiss National Science Foundation; GH and SKh through the SNSF starting grant PRIMA PR00P2.179748 and MC and SKu through Ambizione grant No. 185824.

Nuclear bath		^{13}C	^{13}C	^1H	^1H	^{19}F
		1.1 %	3 to 100 %	biphenyl	Al ₂ O ₃	Al ₂ O ₃
Concentration	n_n (nm^{-3})	1.9	5.1 to 170	41		
	σ_n (nm^{-2})				$\gg 3$	3 [66]
Polarization radius	R_M (nm)	1.33	1.33			
NV center depth	d_{NV} (nm)			6	10	10
Number of nuclei		20	$20 \times \frac{n_c}{n_c^0}$			
Polarization Rate	R (Hz)	9000	9000	7500	375	154
Maximal polarization	p_{max} (%)	> 99	> 99	few %	%	0.3
Diffusion constant	D ($\text{nm}^2 \text{s}^{-1}$)	7 [63]	Eq. (24)	571	700	700
Gyromagnetic ratio	γ_n (MHz T^{-1})	10.7	10.7	42.6	42.6	40.0
Qubit energy	$\varepsilon_{\text{L,R}}$ (MHz)	1.1	1.1	4.4	4.4	4.1
Qubit/bath coupling	$\Gamma_{1,\text{CR}}^{(i)}$ (kHz)	250	Eq. (18)	few 1000	few 1000	few 1000
Decoherence	$\Gamma_2^{(i)}$ (kHz)	1.5 [52]	Eq. (19)	(4.5-14) 10^3	few 100	
Spin-lattice relaxation	$\Gamma_{1,\text{SL}}^{(i)}$ (Hz)	150	150	150	150	150
Reference		[28, 30]		[29]	[30]	[30]

TABLE I. Dynamical Nuclear Polarization parameters for different nuclear spins and concentration. Missing values are either not applicable or not available from the literature

- [1] S. Bravyi, O. Dial, J. M. Gambetta, D. Gil, and Z. Nazario, The future of quantum computing with superconducting qubits, *J. Appl. Phys.* **132**, 160902 (2022).
- [2] C. D. Bruzewicz, J. Chiaverini, R. McConnell, and J. M. Sage, Trapped-ion quantum computing: Progress and challenges, *Appl. Phys. Rev.* **6**, 021314 (2019).
- [3] J. Bohr Brask, G. Haack, N. Brunner, and M. Huber, Autonomous quantum thermal machine for generating steady-state entanglement, *New J. Phys.* **17** (2015).
- [4] A. Tavakoli, G. Haack, M. Huber, N. Brunner, and J. B. Brask, Heralded generation of maximal entanglement in any dimension via incoherent coupling to thermal baths, *Quantum* **2**, 73 (2018).
- [5] A. Tavakoli, G. Haack, N. Brunner, and J. B. Brask, Autonomous multipartite entanglement engines, *Phys. Rev. A* **101**, 012315 (2020).
- [6] S. Khandelwal, N. Palazzo, N. Brunner, and G. Haack, Critical heat current for operating an entanglement engine, *New J. Phys.* **22**, 73039 (2020).
- [7] M. Aguilar, N. Freitas, and J. P. Paz, Entanglement generation in quantum thermal machines, *Phys. Rev. A* **102**, 062422 (2020).
- [8] A. Das, A. A. Khan, S. D. Mishra, P. Solanki, B. De, B. Muralidharan, and S. Vinjanampathy, Steady-state tunable entanglement thermal machine using quantum dots, *Quantum Sci. Technol.* **7**, 045034 (2022).
- [9] M. T. Naseem and Özgür E Müstecaplıoğlu, Engineering entanglement between resonators by hot environment, *Quantum Sci. Technol.* **7**, 045012 (2022).
- [10] J. B. Brask, F. Clivaz, G. Haack, and A. Tavakoli, Operational nonclassicality in minimal autonomous thermal machines, *Quantum* **6**, 672 (2022).
- [11] K. Prech, P. Johansson, E. Nyholm, G. T. Landi, C. Verdozzi, P. Samuelsson, and P. P. Potts, Entanglement and thermokinetic uncertainty relations in coherent mesoscopic transport, *Phys. Rev. Res.* **5**, 023155 (2023).
- [12] A. Gruber, A. Dräbenstedt, C. Tietz, L. Fleury, J. Wrachtrup, and C. V. Borczyskowski, Scanning Confocal Optical Microscopy and Magnetic Resonance on Single Defect Centers, *Science* **276**, 2012 (1997).
- [13] D. Suter, Optical detection of magnetic resonance, *Magnetic Resonance* **1**, 115 (2020).
- [14] H. Babashah, H. Shirzad, E. Losero, V. Goblot, C. Galland, and M. Chipaux, Optically detected magnetic resonance with an open source platform, *arXiv:2205.00005* (2022).
- [15] J. Stortorboom, M. Barbiero, S. Castelletto, and M. Gu, Ground-State Depletion Nanoscopy of Nitrogen-Vacancy Centres in Nanodiamonds, *Nanoscale Res. Lett.* **16**, 44 (2021).
- [16] S. Arroyo-Camejo, M.-P. Adam, M. Besbes, J.-P. Hugonin, V. Jacques, J.-J. Greffet, J.-F. Roch, S. W. Hell, and F. Treussart, Stimulated emission depletion microscopy resolves individual nitrogen vacancy centers in diamond nanocrystals, *ACS Nano* **7**, 10912 (2013).
- [17] G. Balasubramanian, P. Neumann, D. Twitchen, M. Markham, R. Kolesov, N. Mizuochi, J. Isoya, J. Achard, J. Beck, J. Tisler, V. Jacques, P. R. Hemmer, F. Jelezko, and J. Wrachtrup, Ultralong spin coherence time in isotopically engineered diamond, *Nat. Mater.* **8**, 383 (2009).
- [18] L. Rondin, J.-P. Tetienne, T. Hingant, J.-F. Roch, P. Maletinsky, and V. Jacques, Magnetometry with nitrogen-vacancy defects in diamond, *Reports on Progress in Physics* **77**, 056503 (2014).
- [19] J. F. Barry, J. M. Schloss, E. Bauch, M. J. Turner, C. A. Hart, L. M. Pham, and R. L. Walsworth, Sensitivity optimization for NV-diamond magnetometry, *Rev. Mod. Phys.* **92**, 015004 (2020).
- [20] B. Bürgler, T. F. Sjolander, O. Brinza, A. Tal-laire, J. Achard, and P. Maletinsky, All-optical nuclear quantum sensing using nitrogen-vacancy centers in diamond, *npj Quantum Information* **9**, 10.1038/s41534-023-00724-6 (2023).
- [21] K. O. Ho, K. C. Wong, M. Y. Leung, Y. Y. Pang, W. K. Leung, K. Y. Yip, W. Zhang, J. Xie, S. K. Goh, and S. Yang, Recent developments of quantum sensing under pressurized environment using the nitrogen vacancy (NV) center in diamond, *J. Appl. Phys.* **129**, 241101 (2021).
- [22] G. Q. Liu, X. Feng, N. Wang, Q. Li, and R. B. Liu, Coherent quantum control of nitrogen-vacancy center spins near 1000 Kelvin, *Nature Commun.* **10**, 1344 (2019).
- [23] M. Chipaux, K. van der Laan, S. Hemelaar, M. Hasani, T. Zheng, and R. Schirhagl, Nanodiamonds and Their Applications in Cells, *Small* **14**, 1704263 (2018).
- [24] S. Pezzagna and J. Meijer, Quantum computer based on color centers in diamond, *Appl. Phys. Rev.* **8**, 011308 (2021).
- [25] C. Bradley, S. de Bone, P. Möller, S. Baier, M. Degen, S. Loenen, H. Bartling, M. Markham, D. Twitchen, R. Hanson, *et al.*, Robust quantum-network memory based on spin qubits in isotopically engineered diamond, *Npj Quantum Inf.* **8**, 122 (2022).
- [26] M. J. Degen, S. J. Loenen, H. P. Bartling, C. E. Bradley, A. L. Meinsma, M. Markham, D. J. Twitchen, and T. H. Taminiau, Entanglement of dark electron-nuclear spin defects in diamond, *Nature Commun.* **12**, 3470 (2021).
- [27] C. E. Bradley, J. Randall, M. H. Abobeih, R. C. Berrevoets, M. J. Degen, M. A. Bakker, M. Markham, D. J. Twitchen, and T. H. Taminiau, A ten-qubit solid-state spin register with quantum memory up to one minute, *Phys. Rev. X* **9**, 031045 (2019).
- [28] D. A. Broadway, J.-P. Tetienne, A. Stacey, J. D. A. Wood, D. A. Simpson, L. T. Hall, and L. C. L. Hollenberg, Quantum probe hyperpolarisation of molecular nuclear spins, *Nature Commun.* **9**, 1246 (2018).
- [29] A. J. Healey, L. T. Hall, G. A. L. White, T. Teraji, M.-A. Sani, F. Separovic, J.-P. Tetienne, and L. C. L. Hollenberg, Polarization Transfer to External Nuclear Spins Using Ensembles of Nitrogen-Vacancy Centers, *Phys. Rev. Appl.* **10**, 54052 (2021).
- [30] R. Rizzato, F. Bruckmaier, K. S. Liu, S. J. Glaser, and D. B. Bucher, Polarization Transfer from Optically Pumped Ensembles of N-V Centers to Multinuclear Spin Baths, *Phys. Rev. Appl.* **17**, 24067 (2022).
- [31] J.-P. Tetienne, L. T. Hall, A. J. Healey, G. A. L. White, M.-A. Sani, F. Separovic, and L. C. L. Hollenberg, Prospects for nuclear spin hyperpolarization of molecular samples using nitrogen-vacancy centers in diamond, *Phys. Rev. B* **103**, 014434 (2021).

- [32] D. Heineken, K. Beyer, K. Luoma, and W. T. Strunz, Quantum-memory-enhanced dissipative entanglement creation in nonequilibrium steady states, *Phys. Rev. A* **104**, 052426 (2021).
- [33] H.-P. Breuer, F. Petruccione, *et al.*, *The theory of open quantum systems* (Oxford University Press on Demand, 2002).
- [34] H. P. Breuer and F. Petruccione, *The Theory of Open Quantum Systems*, Vol. 1 (Oxford University Press, 2007).
- [35] M. Chipaux, A. Tallaire, J. Achard, S. Pezzagna, J. Meijer, V. Jacques, J.-F. Roch, and T. Debuisschert, Magnetic imaging with an ensemble of nitrogen-vacancy centers in diamond, *Eur. Phys. J. D* **69**, 166 (2015).
- [36] X.-D. Chen, F.-W. Sun, C.-L. Zou, J.-M. Cui, L.-M. Zhou, and G.-C. Guo, Vector magnetic field sensing by a single nitrogen vacancy center in diamond, *Europhys. Lett.* **101**, 67003 (2013).
- [37] D. A. Broadway, J. D. Wood, L. T. Hall, A. Stacey, M. Markham, D. A. Simpson, J.-P. Tetienne, and L. C. Hollenberg, Anticrossing Spin Dynamics of Diamond Nitrogen-Vacancy Centers and All-Optical Low-Frequency Magnetometry, *Phys. Rev. Appl.* **6**, 064001 (2016).
- [38] J. D. Wood, J. P. Tetienne, D. A. Broadway, L. T. Hall, D. A. Simpson, A. Stacey, and L. C. Hollenberg, Microwave-free nuclear magnetic resonance at molecular scales, *Nature Commun.* **8**, 15950 (2017).
- [39] J.-P. P. Tetienne, L. Rondin, P. Spinicelli, M. Chipaux, T. Debuisschert, J.-F. F. Roch, and V. Jacques, Magnetic-field-dependent photodynamics of single NV defects in diamond: An application to qualitative all-optical magnetic imaging, *New J. Phys.* **14**, 103033 (2012).
- [40] M. Auzinsh, A. Berzins, D. Budker, L. Busaite, R. Ferber, F. Gahbauer, R. Lazda, A. Wickenbrock, and H. Zheng, Hyperfine level structure in nitrogen-vacancy centers near the ground-state level anticrossing, *Phys. Rev. B* **100**, 075204 (2019).
- [41] V. Ivády, H. Zheng, A. Wickenbrock, L. Bougas, G. Chatzidrosos, K. Nakamura, H. Sumiya, T. Ohshima, J. Isoya, D. Budker, I. A. Abrikosov, and A. Gali, Photoluminescence at the ground-state level anticrossing of the nitrogen-vacancy center in diamond: A comprehensive study, *Phys. Rev. B* **103**, 035307 (2021).
- [42] A. Dréau, P. Spinicelli, J. R. Maze, J.-F. Roch, and V. Jacques, Single-shot readout of multiple nuclear spin qubits in diamond under ambient conditions, *Phys. Rev. Lett.* **110**, 060502 (2013).
- [43] C. P. Slichter, *Principles of magnetic resonance*, Vol. 1 (Springer Science & Business Media, 2013).
- [44] V. I. Chizhik, Y. S. Chernyshev, A. V. Donets, V. V. Frolov, A. V. Komolkin, and M. G. Shelyapina, *Magnetic resonance and its applications*, Vol. 9783319052991 (springer, 2014).
- [45] E. Dikarov, O. Zgadzai, Y. Artzi, and A. Blank, Direct measurement of the flip-flop rate of electron spins in the solid state, *Phys. Rev. Appl.* **6**, 044001 (2016).
- [46] T. Yamamoto, C. Müller, L. P. McGuinness, T. Teraji, B. Naydenov, S. Onoda, T. Ohshima, J. Wrachtrup, F. Jelezko, and J. Isoya, Strongly coupled diamond spin qubits by molecular nitrogen implantation, *Phys. Rev. B* **88**, 201201(R) (2013).
- [47] I. Jakobi, S. A. Momenzadeh, F. F. De Oliveira, J. Michl, F. Ziem, M. Schreck, P. Neumann, A. Denisenko, and J. Wrachtrup, Efficient creation of dipolar coupled nitrogen-vacancy spin qubits in diamond, *J. Phys. Conf. Ser.* **752** (2016).
- [48] G. Zhao-Jun, C. Xiang-Dong, L. Cong-Cong, L. Shen, Z. Bo-Wen, and S. Fang-Wen, Generation of Nitrogen-Vacancy Center Pairs in Bulk Diamond by Molecular Nitrogen Implantation, *Chin. Phys. Lett.* **33** (2016).
- [49] M. Haruyama, S. Onoda, T. Higuchi, W. Kada, A. Chiba, Y. Hirano, T. Teraji, R. Igarashi, S. Kawai, H. Kawarada, Y. Ishii, R. Fukuda, T. Tanii, J. Isoya, T. Ohshima, and O. Hanaizumi, Triple nitrogen-vacancy centre fabrication by $C_5N_4H_n$ ion implantation, *Nature Commun.* **10**, 2664 (2019).
- [50] S. Pezzagna, B. Naydenov, F. Jelezko, J. Wrachtrup, and J. Meijer, Creation efficiency of nitrogen-vacancy centres in diamond, *New Journal of Physics* **12**, 10.1088/1367-2630/12/6/065017 (2010).
- [51] J. Gugler, T. Astner, A. Angerer, J. Schmiedmayer, J. Majer, and P. Mohn, Ab initio calculation of the spin lattice relaxation time t_1 for nitrogen-vacancy centers in diamond, *Phys. Rev. B* **98**, 214442 (2018).
- [52] N. Mizuochi, P. Neumann, F. Rempp, J. Beck, V. Jacques, P. Siyushev, K. Nakamura, D. Twitchen, H. Watanabe, S. Yamasaki, F. Jelezko, and J. Wrachtrup, Coherence of single spins coupled to a nuclear spin bath of varying density, *Phys. Rev. B* **80**, 41201 (2009).
- [53] N. Bar-Gill, L. M. Pham, A. Jarmola, D. Budker, and R. L. Walsworth, Solid-state electronic spin coherence time approaching one second, *Nature Commun.* **4**, 1743 (2013).
- [54] A. Sigaeva, H. Shirzad, F. P. Martinez, A. C. Nusantara, N. Mougios, M. Chipaux, and R. Schirhagl, Diamond-based nanoscale quantum relaxometry for sensing free radical production in cells, *Small* **18**, 2105750 (2022).
- [55] C. J. Terblanche, E. C. Reynhardt, and J. A. Van Wyk, ^{13}C spin-lattice relaxation in natural diamond: Zeeman relaxation at 4.7 T and 300 K due to fixed paramagnetic nitrogen defects, *Solid State Nucl. Magn. Reson.* **20** (2001).
- [56] J. D. A. Wood, D. A. Broadway, L. T. Hall, A. Stacey, D. A. Simpson, J.-P. Tetienne, and L. C. L. Hollenberg, Wide-band nanoscale magnetic resonance spectroscopy using quantum relaxation of a single spin in diamond, *Phys. Rev. B* **94**, 155402 (2016).
- [57] L. T. Hall, J. H. Cole, and L. C. L. Hollenberg, Analytic solutions to the central-spin problem for nitrogen-vacancy centers in diamond, *Phys. Rev. B* **90**, 075201 (2014).
- [58] S. R. Hartmann and E. L. Hahn, Nuclear double resonance in the rotating frame, *Phys. Rev.* **128**, 2042 (1962).
- [59] F. Shagieva, S. Zaiser, P. Neumann, D. B. R. Dasari, R. Stöhr, A. Denisenko, R. Reuter, C. A. Meriles, and J. Wrachtrup, Microwave-assisted cross-polarization of nuclear spin ensembles from optically pumped nitrogen-vacancy centers in diamond, *Nano Lett.* **18**, 3731 (2018).
- [60] I. Schwartz, J. Scheuer, B. Tratzmiller, S. Müller, Q. Chen, I. Dhand, Z.-Y. Wang, C. Müller, B. Naydenov, F. Jelezko, and M. B. Plenio, Robust optical polarization of nuclear spin baths using hamiltonian engineering of nitrogen-vacancy center quantum dynamics, *Sci. Adv.* **4**, eaat8978 (2018).

- [61] E. Bersin, M. Walsh, S. L. Mouradian, M. E. Trusheim, T. Schröder, and D. Englund, Individual control and readout of qubits in a sub-diffraction volume, **Npj Quantum Inf.** **5**, 38 (2019).
- [62] A. J. Parker, K. Jeong, C. E. Avalos, B. J. Hausmann, C. C. Vassiliou, A. Pines, and J. P. King, Optically pumped dynamic nuclear hyperpolarization in C 13 - enriched diamond, **Phys. Rev. B** **100**, 041203(R) (2019).
- [63] A. Ajoy, B. Safvati, R. Nazaryan, J. T. Oon, B. Han, P. Raghavan, R. Nirodi, A. Aguilar, K. Liu, X. Cai, X. Lv, E. Druga, C. Ramanathan, J. A. Reimer, C. A. Meriles, D. Suter, and A. Pines, Hyperpolarized relaxometry based nuclear T_1 noise spectroscopy in diamond, **Nature Commun.** **10**, 5160 (2019).
- [64] S. Khandelwal, N. Brunner, and G. Haack, Signatures of liouvillian exceptional points in a quantum thermal machine, **PRX Quantum** **2**, 040346 (2021).
- [65] W. K. Wootters, Entanglement of formation of an arbitrary state of two qubits, **Phys. Rev. Lett.** **80**, 2245 (1998).
- [66] K. S. Liu, A. Henning, M. W. Heindl, R. D. Allert, J. D. Bartl, I. D. Sharp, R. Rizzato, and D. B. Bucher, Surface nmr using quantum sensors in diamond, **Proc. Natl. Acad. Sci. U.S.A.** **119**, e2111607119 (2022).
- [67] R. J. de Assis, T. M. de Mendonça, C. J. Villas-Boas, A. M. de Souza, R. S. Sarthour, I. S. Oliveira, and N. G. de Almeida, Efficiency of a quantum otto heat engine operating under a reservoir at effective negative temperatures, **Phys. Rev. Lett.** **122**, 240602 (2019).
- [68] J. Nettersheim, S. Burgardt, Q. Bouton, D. Adam, E. Lutz, and A. Widera, Power of a quasispin quantum otto engine at negative effective spin temperature, **PRX Quantum** **3**, 040334 (2022).